Article

Preparation of Pd/SiO$_2$ Catalysts by a Simple Dry Ball-Milling Method for Lean Methane Oxidation and Probe of the State of Active Pd Species

Li Yang [1,2], Chao Fan [1,2], Li Luo [1,2], Yanyan Chen [1], Zhiwei Wu [1,*], Zhangfeng Qin [1,*], Mei Dong [1], Weibin Fan [1] and Jianguo Wang [1,2,*]

[1]   State Key Laboratory of Coal Conversion, Institute of Coal Chemistry, Chinese Academy of Sciences, Taiyuan 030001, China; yangli1151@hotmail.com (L.Y.); fanchao@sxicc.ac.cn (C.F.); luoli@sxicc.ac.cn (L.L.); chenyanyan@sxicc.ac.cn (Y.C.); mdong@sxicc.ac.cn (M.D.); fanwb@sxicc.ac.cn (W.F.)
[2]   University of the Chinese Academy of Sciences, Beijing 100049, China
*   Correspondence: wuzhiwei@sxicc.ac.cn (Z.W.); qzhf@sxicc.ac.cn (Z.Q.); iccjgw@sxicc.ac.cn (J.W.); Tel.: +86-351-4046092 (Z.Q. & Z.W. & J.W.); Fax: +86-351-4041153 (Z.Q. & Z.W. & J.W.)

Abstract: A series of Pd/SiO$_2$ catalysts were prepared with different Pd precursors by a dry ball-milling method and used in the catalytic oxidation of lean methane at low temperature. The effect of Pd precursors on the catalytic performance was investigated and the state of the most active Pd species was probed. The results indicate that dry ball-milling is a simple but rather effective method to prepare the Pd/SiO$_2$ catalysts for lean methane oxidation, and palladium acetylacetonate is an ideal precursor to obtain a highly active Pd/SiO$_2$-Acac catalyst with well- and stably dispersed Pd species, owing to the tight contact between acetylacetonate and Si–OH on the SiO$_2$ support. Besides the size and dispersion of Pd particles, the oxidation state of Pd species also plays a crucial role in determining the catalytic activity of Pd/SiO$_2$ in lean methane oxidation at low temperature. A non-monotonic dependence of the catalytic activity on the Pd oxidation state is observed. The activity of various Pd species follows the order of PdO$_x$ >> Pd > PdO; the PdO$_x$/SiO$_2$-Acac catalysts (in particular for PdO$_{0.82}$/SiO$_2$-Acac when $x = 0.82$) exhibit much higher activity in lean methane oxidation at low temperature than Pd/SiO$_2$-Acac and PdO/SiO$_2$-Acac. The catalytic activity of PdO$_x$/SiO$_2$ may degrade during the methane oxidation due to the gradual transformation of PdO$_x$ to PdO in the oxygen-rich ambiance; however, such degradation is reversible and the activity of a degraded Pd/SiO$_2$ catalyst can be recovered through a redox treatment to regain the PdO$_x$ species. This work helps to foster a better understanding of the relationship between the structure and performance of supported Pd catalysts by clarifying the state of active Pd species, which should be beneficial to the design of an active catalyst in lean methane oxidation at low temperature.

Keywords: lean methane mitigation; catalytic oxidation; Pd/SiO$_2$; ball-milling method; active Pd species

1. Introduction

As the second most important gas after carbon dioxide that contributes to the greenhouse effect, anthropogenic methane emissions, mostly in a low concentration of about 0.1–1.0 vol.%, have caused serious environmental problems [1,2]. Catalytic oxidation at low temperature is regarded as an effective measure in the mitigation of lean methane emission and the recovery of wasted energy. Among multifarious catalysts tested, the supported Pd, in particular on silica-based materials, was a group of the most widely used and extensively studied catalysts in lean methane oxidation over the past few decades [3–6]. However, the search for a more efficient catalyst in lean methane oxidation and a better preparation method remains a great challenge due to the chemical inertness of methane.

Although a great deal of effort has been made to correlate the catalytic performance with the state and size of the Pd component and reaction atmosphere, there is still considerable controversy on the state of the most active Pd species as well as the size effect of supported Pd particles [7–10]. Various Pd species, including bulk PdO [5], metallic Pd [9], Pd oxide covered on metallic Pd [11,12], and the co-existence of Pd and PdO [13], have been attributed to the most active sites in lean methane oxidation. As the lean methane oxidation is in general conducted in an oxygen-excessive ambiance and the active metal species on the catalysts were often subjected to oxidation prior to reaction, a direct comparison was rarely made between the reduced and oxidized Pd species [14]. Su and co-workers reported that methane decomposition did not readily occur on PdO and there was an induction period in which PdO was reduced to Pd nuclei by methane [4]. Xiong and co-workers investigated the effect of the Pd oxidation state on the oxidation of methane, propane and propylene and found that metallic Pd was more active than PdO [15]; when the reduced catalyst was tested under lean fuel conditions, the catalytic activity declined due to the formation of PdO. By using Operando XANES conducted at Beamline ID24 of the European Synchrotron Radiation Facility in Grenoble, France, Nilsson and co-workers found that switching off oxygen led to a transformation of PdO to metal Pd except at a low temperature, where such a phase transformation was very slow [13]. Interestingly, they observed that the highest catalytic activity for methane oxidation was obtained when oxygen was switched off, implying that the co-existence of metallic Pd and PdO was probably essential to achieve high reactivity at a low temperature. However, it is often rather difficult to determine the active state of Pd species, as metal Pd could be converted into PdO under oxygen-excessive ambiance at a moderate temperature; actually, there were few detailed reports on the nature of active Pd sites in a working catalyst for lean methane oxidation.

Nevertheless, as the transformation of metal Pd to PdO (perhaps via an intermediate such as a layer of PdO covered on Pd) is relatively slow at a low temperature, it is possible to find a kinetic zone to observe the effect of such a transformation on the catalytic activity in methane oxidation. Doan and co-workers reported that for methane oxidation, methane was preferentially dissociatively adsorbed on metallic Pd and then oxidized by the PdO species [16]; the catalytic activity of Pd/ZrO_2 increased up to a maximum with an increase in the proportion of surface PdO. Burch and co-workers also observed that the activity of supported Pd catalysts increased until an optimum oxide coverage of approximately 3–4 monolayers [17]. Lin and co-workers also reported similar findings over a pre-oxidized $Pd/TiO_2/Al_2O_3$ catalyst [18].

Among a large variety of catalyst preparation approaches, incipient impregnation is probably the most popular way to obtain the supported metal catalysts; however, the impregnation method may produce waste water as well as harmful emissions due to the evaporation of solvent and/or decomposition of metal precursors upon later drying and calcination treatments. In contrast, mechanochemical measures such as grinding and ball-milling are rather old and simple methods to prepare catalysts, which is realized just through mixing different components together and can ensure a lower impact on the ambient environment. Meanwhile, for the preparation of supported Pd catalysts, various precursors, including palladium chloride ($PdCl_2$), nitrate ($Pd(NO_3)_2$), acetate ($Pd(OAc)_2$) and acetylacetonate ($Pd(Acac)_2$), are available. Palladium chloride and nitrate are somewhat more stable and cheaper, but the Pd catalysts prepared with chloride and nitrate as precursors may keep certain chlorine residual and/or emit noxious and pungent gases upon later thermal treatment. In contrast, palladium acetate and acetylacetonate are probably more appropriate precursors to prepare the supported Pd catalysts with high dispersion [19–25]. By mixing $Pd(OAc)_2$ with CeO_2 polycrystalline powder in a dry way, the Pd–O–Ce interface was obtained, with the Pd moieties partially embedded in the outer surface layers of ceria [23]; the resultant Pd/CeO_2 catalyst showed a much lower temperature in methane activation compared to conventional catalysts. EXAFS and DRIFT results indicated that the dispersion of organic palladium complex $Pd(Acac)_2$ adsorbed on

the support is related to the nature of the support surface [24]: molecular level dispersion was observed on MgO, whereas islands of multilayers were formed on SiO_2. In addition, due to the presence of –OH groups on the SiO_2 support surface, hydrogen transfer from the surface hydroxyls to the acetylacetonate ligand could be observed [25].

To search for more a efficient method to prepare active catalyst in the lean methane oxidation at low temperature as well as to foster a better understanding of the relationship between the structure and performance of supported Pd catalysts, in this work, a series of Pd/SiO_2 catalysts (Pd/SiO_2-*R*, where *R* is Cl, NO_3, OAc and Acac, representing $PdCl_2$, $Pd(NO_3)_2$, $Pd(OAc)_2$ and $Pd(Acac)_2$, respectively, as the Pd precursor) were prepared by a simple dry ball-milling method, as specified later in the experimental section. The effect of Pd precursors on the catalytic performance as well as the state of the most active Pd species was investigated, through a cooperative regulation and probe of the oxidation state of Pd species as well as an elaborate correlation of the catalytic performance with the Pd oxidation state.

2. Results and Discussion

2.1. Effect of the Pd Precursor on the Structural Properties of Pd/SiO₂ Catalyst

Table 1 gives the basic structural properties of Pd/SiO_2 catalysts prepared by the dry ball-milling method with different Pd precursors. Obviously, all the Pd/SiO_2 catalysts display a similar surface area rather close to that of the SiO_2 support, suggesting that such a mechanical milling mixing method has little impact on the textural structure of the pristine SiO_2 support. In addition, the actual Pd loading of all the Pd/SiO_2 catalysts measured by ICP-OES is approximately equal to the designated value, proving that it is able to avoid any material loss by using the mechanical mixing method to prepare the Pd/SiO_2 catalysts. In contrast, four Pd/SiO_2 catalysts are rather different in the size of Pd particles reflecting the Pd dispersion, as shown in Figure 1, Table 1 and Figure S1 of the Supplementary Materials. That is, the precursor used to carry Pd has a significant influence on the Pd particle size of resultant catalysts; for the Pd/SiO_2 catalysts calcined at 400 °C and reduced at 400 °C, palladium acetate ($Pd(OAc)_2$) and in particular acetylacetonate ($Pd(Acac)_2$) give much smaller Pd particles (7.7 and 4.6 nm, respectively), whereas palladium chloride ($PdCl_2$) and nitrate ($Pd(NO_3)_2$) lead to much larger Pd particles (12.3 and 14.5 nm, respectively).

Table 1. Structural properties of the Pd/SiO_2 catalysts prepared by the dry ball-milling method with different Pd precursors.

Catalyst	Pd Precursor	Pd Loading (wt.%)	Surface Area ($m^2 g^{-1}$)	Pd Particle Size (nm)
SiO_2	none	0	194	
Pd/SiO_2-Acac	$Pd(Acac)_2$	1.00	192	4.6
Pd/SiO_2-OAc	$Pd(OAc)_2$	1.02	195	7.7
Pd/SiO_2-Cl	$PdCl_2$	0.98	192	12.3
Pd/SiO_2-NO_3	$Pd(NO_3)_2$	1.03	193	14.5

Note: After the dry ball-milling of fumed silica (SiO_2) together with Pd precursor for 1 h, the Pd/SiO_2-*R* catalysts was calcined in air at 400 °C for 4 h and then reduced with hydrogen at 400 °C for 1 h. The actual Pd loading was measured by ICP-OES. The surface area was determined by BET method from the nitrogen adsorption isotherms. The average size of Pd particles was estimated from the TEM images (Figure 1).

Moreover, as shown in Figure 1 and Figure S1, for the Pd/SiO_2-Acac and Pd/SiO_2-OAc catalysts, the calcination treatment at 400–800 °C as well as reduction at 400 °C does not induce any marked agglomeration of Pd species and the increase in Pd particle size upon these calcination and reduction treatments is also rather insignificant. In contrast, a marked increase in the Pd particle size was observed on the Pd/SiO_2-Cl and Pd/SiO_2-NO_3 catalysts upon calcination at elevated temperature. The current results illustrate that the Pd particle size or Pd dispersion of the Pd/SiO_2 catalyst prepared by the dry ball-milling method is closely related to the Pd precursor; with palladium acetylacetonate as the precursor, the Pd/SiO_2-Acac catalyst displays a high dispersion of Pd species as

well as a superior resistance against sintering upon calcination and reduction at a relatively high temperature.
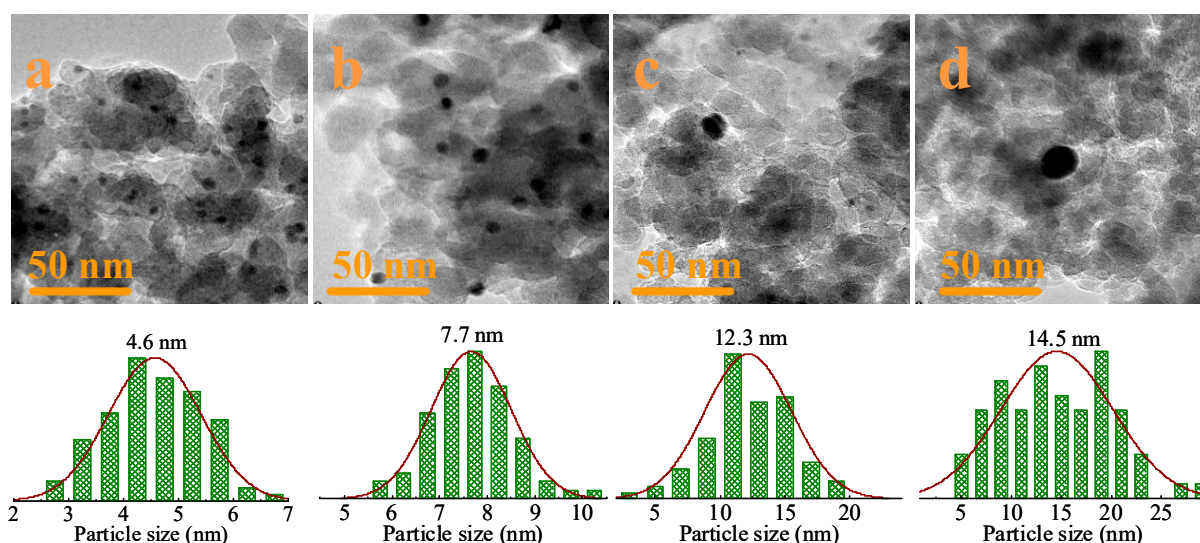

Figure 1. TEM images and Pd particle size distribution curves of the Pd/SiO$_2$-*R* catalysts prepared by the dry ball-milling method with different Pd precursors (after the dry ball-milling of fumed silica (SiO$_2$) together with Pd precursor for 1 h, the Pd/SiO$_2$-*R* catalysts was calcined in air at 400 °C for 4 h and then reduced with hydrogen at 400 °C for 1 h): (**a**) Pd/SiO$_2$-Acac, (**b**) Pd/SiO$_2$-OAc, (**c**) Pd/SiO$_2$-Cl, and (**d**) Pd/SiO$_2$-NO$_3$.

The evolution of the mixture of SiO$_2$ support and different Pd precursors from the dry ball-milling upon later calcination at elevated temperatures were explored by in situ XRD, as demonstrated in Figure 2. After the ball-milling, no diffraction lines are observed for Pd(Acac)$_2$/SiO$_2$ and Pd(OAc)$_2$/SiO$_2$ at 30 °C, suggesting that the Pd(Acac)$_2$ and Pd(OAc)$_2$ precursors are well dispersed on the SiO$_2$ support. Pd(Acac)$_2$ and Pd(OAc)$_2$ on SiO$_2$ start to decompose at a temperature above 150 °C, as evidenced by the appearance of diffraction lines for metallic Pd in the XRD patterns of Pd(Acac)$_2$/SiO$_2$ and Pd(OAc)$_2$/SiO$_2$ calcined at 150 °C. When the calcination temperature is elevated to above 300 °C, the diffraction peaks attributed to PdO begin to emerge and the diffraction intensity of PdO increases gradually with the increase in calcination temperature, indicating the agglomeration of PdO on Pd/SiO$_2$-Acac and Pd/SiO$_2$-OAc. As the Pd species are well dispersed on Pd(Acac)$_2$/SiO$_2$, the diffraction lines of either Pd or PdO on the low-temperature calcined Pd(Acac)$_2$/SiO$_2$ catalyst are rather weak.

In contrast, the diffraction lines for PdCl$_2$ and PdO are detected for PdCl$_2$/SiO$_2$ and Pd(NO$_3$)$_2$/SiO$_2$, respectively, even at 30 °C, implying that it is somewhat difficult to obtain highly dispersed PdCl$_2$ and Pd(NO$_3$)$_2$ just through the mechanical ball-milling. The diffraction line of PdCl$_2$ is replaced by the diffraction peaks of PdO phase for the PdCl$_2$/SiO$_2$ catalyst calcined above 400 °C. After that, for all the Pd/SiO$_2$-*R* catalysts, the intensity of diffraction peaks attributed to PdO increases with increasing the calcination temperature due to the agglomeration of PdO, although four Pd/SiO$_2$ catalysts are rather different in the agglomeration degree, consistent with the TEM results.

It is especially noteworthy that among four Pd precursors used in this work, Pd(Acac)$_2$ always gives the Pd/SiO$_2$-Acac catalyst the highest dispersion of Pd species and superior resistance against sintering upon calcination and reduction at high temperature. As reported by Van Veen and co-workers, for the thermal decomposition of supported metal acetylacetonate complexes (M(Acac)$_n$) on the SiO$_2$ support, the transfer of H from surface –OH groups to adsorbed M(Acac)$_n$ to form Acac–H was consistently observed [25]. As shown in Figure S2 of the Supplementary Materials, an absorption peak at 960 cm^{-1} assigned to the Si–OH asymmetric stretching vibrations is observed in the FT-IR spectrum of the SiO$_2$ support [26]; this characteristic peak of Si–OH becomes much weaker in the

spectrum of Pd/SiO-Acac loaded with the Pd(acac)$_2$ precursor, indicating the formation of Acac-H. At the same time, the palladium species was reduced to highly dispersed metallic Pd (with very weak diffraction signals in Figure 2) by the Acac ligand at elevated temperature (about 200 °C). In addition, the TG-MS curves shown in Figure S3 of the Supplementary Materials also illustrate that there is a steep weight loss at 198 °C for Pd(Acac)$_2$/SiO$_2$, accompanied with a sharp DTG peak as well as sharp mass spectroscopy signals for CO$_2$ and H$_2$O, indicating the thermal decomposition of Acac ligands supported on SiO$_2$, consistent with the in situ XRD results (Figure 2).
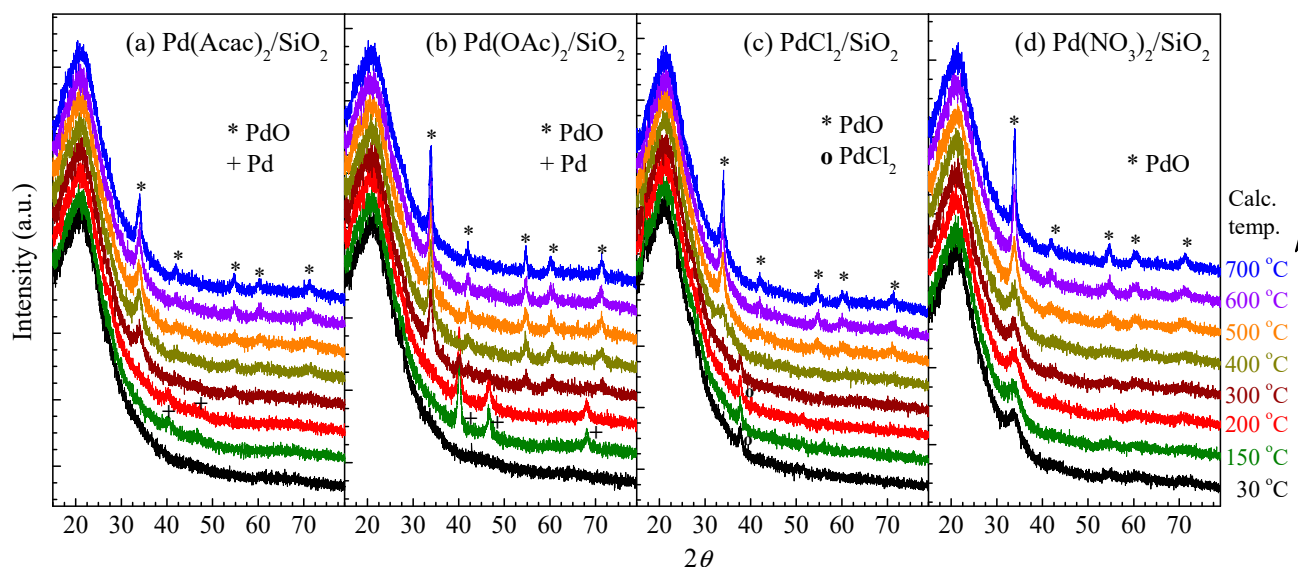

Figure 2. XRD patterns of the mixture of SiO$_2$ support + different Pd precursors from dry ball-milling, collected after calcination at step-wise elevated temperatures (from bottom up, corresponding to 30, 150, 200, 300, 400, 500, 600 and 700 °C in sequences, as marked right in the legend): (**a**) Pd(Acac)$_2$/SiO$_2$, (**b**) Pd(OAc)$_2$/SiO$_2$, (**c**) PdCl$_2$/SiO$_2$, and (**d**) Pd(NO$_3$)$_2$/SiO$_2$.

2.2. Performance of the Pd/SiO$_2$ Catalysts Prepared by the Dry Ball-Milling Method in Lean Methane Oxidation

The overall performance of various Pd/SiO$_2$-R catalysts prepared by the dry ball-milling method with different Pd precursors in the lean methane oxidation was compared by the light-off tests, as shown in Figure 3A and Figure S4 of the Supplementary Materials. Apparently, four Pd/SiO$_2$ catalysts prepared with different Pd precursors are also rather different in the catalytic activity for methane oxidation. The Pd/SiO$_2$-Acac catalyst prepared with palladium acetylacetonate performs the best in lean methane oxidation; the temperatures corresponding to a methane conversion of 10% ($T_{10\%}$), 50% ($T_{50\%}$) and 90% ($T_{90\%}$) are 242, 272 and 288 °C, respectively, and a complete methane conversion ($T_{100\%}$) is achieved at about 310 °C. Next is the Pd/SiO$_2$-OAc catalyst prepared from palladium acetate, with $T_{10\%}$, $T_{50\%}$, $T_{90\%}$ and $T_{100\%}$ values of 245, 280, 305 and 335 °C, respectively. The third is the Pd/SiO$_2$-Cl catalyst prepared from palladium chloride, with a $T_{90\%}$ value of 345 °C. The Pd/SiO$_2$-NO$_3$ catalyst prepared from palladium nitrate performs poorest, with a $T_{90\%}$ value of 464 °C. That is, the catalytic activity of various Pd/SiO$_2$ catalysts follows the order of Pd/SiO$_2$-Acac > Pd/SiO$_2$-OAc > Pd/SiO$_2$-Cl >> Pd/SiO$_2$-NO$_3$; such an order of catalytic activity in methane oxidation is consistent with that of Pd dispersion or Pd particle size [9]; that is, the catalytic activity increases with an increase in the Pd dispersion or a decrease in the Pd particle size.
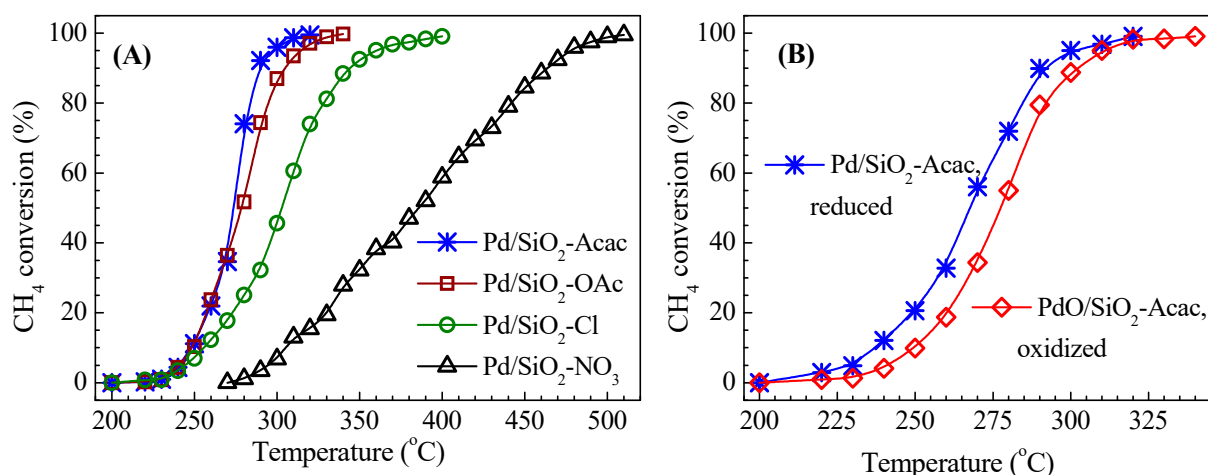
Figure 3. (**A**) A comparison of the Pd/SiO_2-R catalysts prepared by the dry ball-milling method with different Pd precursors in their activity for lean methane oxidation. After the dry ball-milling, the Pd/SiO_2-R catalysts were calcined in air at 400 °C for 4 h and then reduced with hydrogen at 400 °C for 1 h. (**B**) A comparison of the Pd/SiO_2-Acac (reduced) and the PdO/SiO_2-Acac (oxidized) catalysts of different Pd oxidation states in their activity for lean methane oxidation. The light-off reaction tests were conducted with the feed of 1 vol.% CH_4 and 99 vol.% air and a GHSV of 30,000 mL h^{-1} g^{-1}.

Interestingly, as shown in Figure S4, four Pd/SiO_2-R catalysts prepared from different Pd precursors are also rather different in the thermal stability against calcination treatment at elevated temperatures. For the Pd/SiO_2-Acac catalyst, it seems that the calcination at a temperature below 800 °C has little impact on its catalytic activity in methane oxidation, according well with its superior resistance against sintering upon calcination at elevated temperatures. In contrast, the Pd/SiO_2-OAc catalyst displays a moderate decrease in the activity for methane oxidation upon calcination at a temperature higher than 600 °C, whereas such a calcination treatment has a significant detrimental influence on the catalytic activity of Pd/SiO_2-Cl and Pd/SiO_2-NO_3 in lean methane oxidation, in accordance with the serious agglomeration of Pd species on Pd/SiO_2-Cl and Pd/SiO_2-NO_3 at elevated temperatures, as demonstrated by the XRD and TEM results (Figure 2 and Figure S1). Besides the catalytic activity, the thermal stability of Pd/SiO_2 catalysts also follows the order of Pd/SiO_2-Acac > Pd/SiO_2-OAc >> Pd/SiO_2-Cl > Pd/SiO_2-NO_3, indicating that palladium acetylacetonate is an appropriate precursor, much superior to palladium acetate, chloride and nitrate, to prepare the Pd/SiO_2 catalyst with high activity and stability for lean methane oxidation through the dry ball-milling method.

In addition, a rough comparison of current Pd/SiO_2-Acac catalyst with some other supported palladium catalysts in their activity for lean methane oxidation was given in Table S1 of the Supplementary Materials. Obviously, current Pd/SiO_2-Acac catalyst prepared by the simple dry ball-milling method exhibits rather high activity in the lean methane oxidation, compared with most of those catalysts reported in the open literature.

2.3. Effect of Pd Chemical State on the Catalytic Activity of Pd/SiO₂ in Lean Methane Oxidation

The activity of Pd/SiO_2-Acac catalyst in reduced state and the PdO/SiO_2-Acac catalyst in oxidized state in lean methane oxidation is compared in Figure 3B. Obviously, the oxidation state of Pd species does have a certain influence on the catalytic activity of PdO/SiO_2. The PdO/SiO_2-Acac catalyst in oxidized state (calcined at 400 °C, with a $T_{90\%}$ value of 313 °C) exhibits a lower activity than the Pd/SiO_2-Acac catalyst in reduced state (reduced at 400 °C, with a $T_{90\%}$ value of 287 °C). It suggests that Pd^0 on the supported Pd/SiO_2 catalyst is more active than PdO for the lean methane oxidation. However, it is noteworthy that during the light-off tests for methane oxidation, oxygen is always highly excessive and the reduced Pd^0 species could be oxidized to PdO in the oxygen-rich ambiance (the oxygen concentration in the reaction stream is in general higher than 18 vol.%) at elevated temperatures. This is proved by the in situ XRD patterns of the

Pd/SiO_2-Acac catalysts that come through the lean methane oxidation reaction at different temperatures, as shown in Figure S5A of the Supplementary Materials. It means that the actual working Pd species in lean methane oxidation may include the PdO_x species even when the reduced Pd/SiO_2 catalyst with only Pd^0 species is initially used. Moreover, it seems that the content of PdO increases with the increase in reaction temperature and the PdO species rather than Pd^0 turns out to be the primary Pd species for lean methane oxidation at a temperature above 320 °C.

To evaluate the effect of the Pd chemical state on the catalytic activity of Pd/SiO_2 in lean methane oxidation, various Pd/SiO_2-Acac catalysts with different Pd oxidation states were tested at a fixed low temperature of 230 °C. As demonstrated in Figure S5A, a temperature below 240 °C for the lean methane oxidation does not induce a serious transformation of the Pd^0 species to PdO in a certain reaction period (about several hours).

A series of PdO_x/SiO_2-Acac catalysts was first prepared by oxidizing the previously reduced Pd/SiO_2-Acac in air for 30 min at different temperatures (240–500 °C), which was then characterized by Pd 3d XPS to determine the value of x = [PdO]/([Pd] + [PdO]), as illustrated in Table 2 and Figure S6 of the Supplementary Materials. The TEM images shown in Figure S7 of the Supplementary Materials illustrate that such an oxidation treatment at 240–500 °C has little impact on the catalyst morphology and Pd dispersion; all the PdO_x/SiO_2-Acac catalysts in this series have a similar Pd particle size, in the range of 4.2–4.8 nm, as given in Table 2.

Table 2. PdO_x/SiO_2-Acac catalysts with different Pd oxidation states, related to oxidation temperature and performance in lean methane oxidation.

Catalysts	Oxidation Temperature (°C)	Pd Particle Size (nm)	x, PdO/(Pd + PdO)	Methane Conversion (%)	TOF (h^{-1})
Pd/SiO_2-Acac	reduced	4.6	0	1.0	1.4
$PdO_{0.36}/SiO_2$-Acac	240	4.7	0.36	3.0	4.3
$PdO_{0.58}/SiO_2$-Acac	250	4.8	0.58	4.6	6.6
$PdO_{0.75}/SiO_2$-Acac	300	4.5	0.75	4.9	7.0
$PdO_{0.82}/SiO_2$-Acac	350	4.5	0.82	5.5	7.8
$PdO_{0.88}/SiO_2$-Acac	400	4.7	0.88	4.3	6.1
$PdO_{0.95}/SiO_2$-Acac	500	4.6	0.95	1.8	2.6
PdO/SiO_2-Acac	calcined	4.2	1	0.5	0.7

Note: The PdO_x/SiO_2-Acac catalysts with different Pd oxidation states were prepared by oxidizing the previously reduced Pd/SiO_2-Acac for 30 min at different temperatures, as specified in column 2. The value of x = [PdO]/([Pd] + [PdO] in column 4 is determined by the Pd 3d XPS (Figure S6 of the Supplementary Materials). The Pd particle size was estimated from the TEM images (Figure S7 of the Supplementary Materials). The conversion of methane and turnover frequency (TOF) was measured at a fixed reaction temperature of 230 °C with the feed of 1 vol.% CH_4 and 99 vol.% air and a GHSV of 30,000 mL h^{-1} g^{-1}.

When this series of PdO_x/SiO_2-Acac catalysts is employed in the lean methane oxidation, as shown in Figure 4A,C, the catalytic activity is closely connected with the oxidation state of Pd species (represented by the value of x). It seems that PdO/SiO_2-Acac (x = 1) has the lowest activity (with a turnover frequency (TOF) of 0.7 h^{-1}) and Pd/SiO_2-Acac (x = 0) shows slightly higher activity (with a TOF of 1.4 h^{-1}) than PdO/SiO_2-Acac. In contrast, the PdO_x/SiO_2-Acac catalysts (x = 0.36–0.95) exhibit much higher activity for the lean methane oxidation at low temperature (230 °C). That is, the activity of various Pd species follows the order of $PdO_x \gg Pd > PdO$. In particular, the $PdO_{0.82}/SiO_2$-Acac catalyst is most active, with the highest TOF (7.8 h^{-1}) and methane conversion (5.5%).

Next, to help reveal the nature of the PdO_x species on Pd/SiO_2, another series of xPdO + (1 − x)Pd/SiO_2-Acac catalysts (x = 0–1) was prepared by mixing the reduced (1 − x)Pd/SiO_2-Acac portion and oxidized xPdO/SiO_2-Acac portion through grinding; both the Pd and PdO phases could be detected in their XRD patterns, as shown in Figure S5B of the Supplementary Materials. When this series of xPdO + (1 − x)Pd/SiO_2-Acac catalysts

is tested in lean methane oxidation, as shown in Figure 4B,C, the xPdO + $(1 − x)$Pd/SiO$_2$-Acac catalysts (x = 0.2, 0.4, 0.6 and 0.8) show similar activity to PdO/SiO$_2$-Acac and Pd/SiO$_2$-Acac (with the TOF of 1–2 h$^{−1}$); in most cases, slightly more active than Pd/SiO$_2$-Acac and less active than PdO/SiO$_2$-Acac. It indicates that a simple mixing of the reduced Pd/SiO$_2$-Acac and oxidized PdO/SiO$_2$-Acac catalysts does not give any synergy between the Pd^0 and PdO species in two catalysts for the lean methane oxidation. The high catalytic activity of PdO$_x$/SiO$_2$-Acac should be related to its particular structure and properties with a tight interaction between the Pd atoms of different valence states.

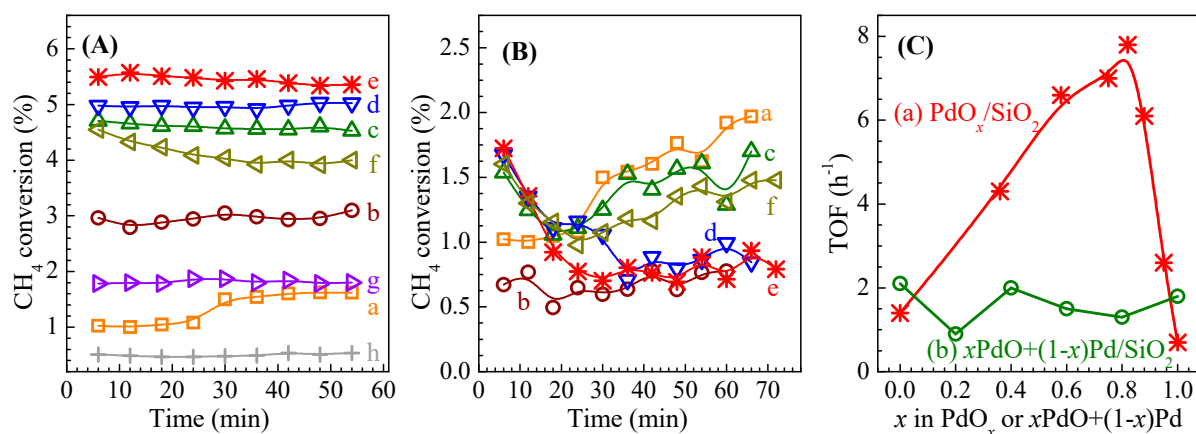**Figure 4.** Lean methane oxidation at 230 °C over the Pd/SiO$_2$-Acac catalysts with different Pd oxidation states. (**A**) Methane conversion versus reaction time over the PdO$_x$/SiO$_2$-Acac series catalysts: (**a**) Pd/SiO$_2$-Acac; (**b**) PdO$_{0.36}$/SiO$_2$-Acac; (**c**) PdO$_{0.58}$/SiO$_2$-Acac; (**d**) PdO$_{0.75}$/SiO$_2$-Acac; (**e**) PdO$_{0.82}$/SiO$_2$-Acac; (**f**) PdO$_{0.88}$/SiO$_2$-Acac; (**g**) PdO$_{0.95}$/SiO$_2$-Acac; (**h**) PdO/SiO$_2$-Acac. (**B**) Methane conversion versus reaction time over the xPdO + $(1 − x)$Pd/SiO$_2$-Acac series catalysts: (**a**) Pd/SiO$_2$-Acac; (**b**) 0.2 PdO + 0.8 Pd/SiO$_2$-Acac; (**c**) 0.4 PdO + 0.6 Pd/SiO$_2$-Acac; (**d**) 0.6 PdO + 0.4 Pd/SiO$_2$-Acac; (**e**) 0.8 PdO + 0.2 Pd/SiO$_2$-Acac; (**f**) PdO/SiO$_2$-Acac. (**C**) Turnover frequency (TOF, as specified later in the experimental section) versus the value of x in the PdO$_x$/SiO$_2$-Acac series (**a**) or the xPdO + $(1 − x)$Pd/SiO$_2$-Acac series (**b**) catalysts. The reactions were conducted at 230 °C, with the feed of 1 vol.% CH$_4$ and 99 vol.% air and a GHSV of 30,000 mL h$^{−1}$ g$^{−1}$.

The H$_2$-TPR profiles of PdO$_x$/SiO$_2$-Acac with different x values are presented in Figure 5A. Two intense peaks are observed; a hydrogen consumption peak at −10–40 °C probably involves a superposition of the reduction of PdO species to the metal Pd^0 species and the formation of palladium hydride (PdH$_x$) from the Pd^0 species, whereas another is a hydrogen desorption peak at 45–75 °C, corresponding to the decomposition of palladium hydride [27]. As shown in Figure 5A, the PdO/SiO$_2$-Acac catalyst displays the highest reduction temperature compared to the PdO$_x$/SiO$_2$-Acac catalysts. In particular, the PdO$_{0.82}$/SiO$_2$-Acac catalyst shows the lowest reduction temperature, indicating a superior reducibility, which allows a quick redox cycle and then gives it a high activity for the lean methane oxidation at low temperature.

A long-term catalytic test was then performed for the lean methane oxidation over the PdO$_{0.82}$/SiO$_2$-Acac catalyst at 280 °C, as shown in Figure 5B. Obviously, the catalytic activity of PdO$_{0.82}$/SiO$_2$-Acac is degraded gradually with the time on stream; the fresh PdO$_{0.82}$/SiO$_2$-Acac catalyst shows a methane conversion of 49.6%, which decreases to 28.1% after reaction at 280 °C for 60 h. However, when the degraded PdO$_{0.82}$/SiO$_2$-Acac catalyst is re-treated according to the procedures for preparing the fresh PdO$_{0.82}$/SiO$_2$-Acac catalyst (viz., reduced by H$_2$ at 400 °C for 1 h and re-oxidized by air at 350 °C for 0.5 h), the activity of the degraded PdO$_{0.82}$/SiO$_2$-Acac catalyst is completely recovered and the conversion of methane comes back to 50.2%.

For the supported palladium catalysts in lean methane oxidation, the degradation of catalytic activity may stem from two main causes: state transformation of active Pd species and the sintering of Pd particles. In comparison with the fresh PdO$_{0.82}$/SiO$_2$-Acac catalyst, after enduring the lean methane oxidation at 280 °C for 60 h, as shown in Figure S8 of the

Supplementary Materials, no significant change in the catalyst morphology and Pd particle size is observed on the spent $PdO_{0.82}/SiO_2$-Acac catalyst by the TEM images, whereas the chemical state of Pd changes from $PdO_{0.82}/SiO_2$ to PdO/SiO_2, as evidenced by the Pd 3d XPS spectra. These results indicate that the degradation of $PdO_{0.82}/SiO_2$-Acac in catalytic activity during the lean methane oxidation at low temperature is primarily ascribed to the over oxidation of PdO_x species, rather than any change in the Pd particle size; nevertheless, such a degradation process is reversible and the reactivity of the degraded $PdO_{0.82}/SiO_2$-Acac catalyst can be completely recovered when the oxidation state of Pd species is resumed to original $PdO_{0.82}$ through proper redox treatments.
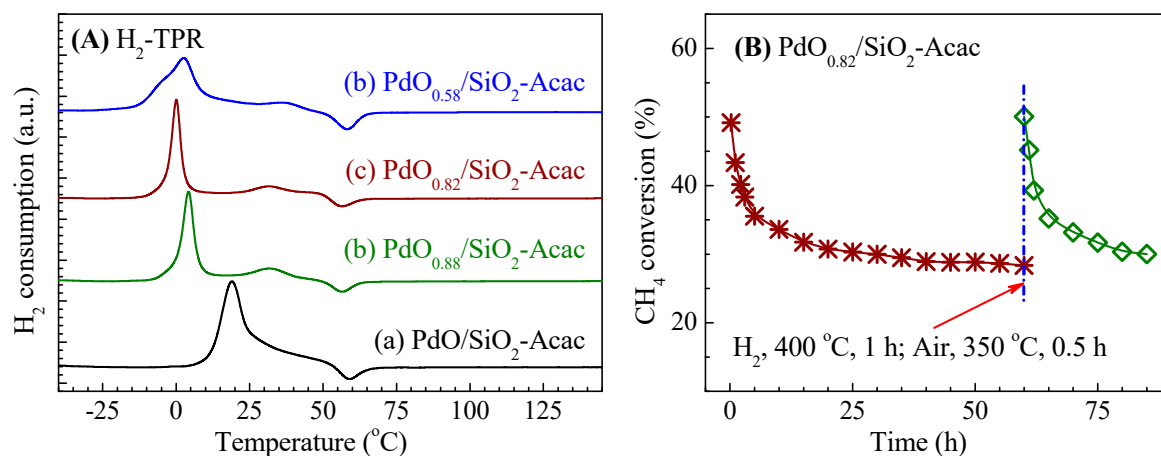

Figure 5. (**A**) H_2-TPR profiles of (**a**) PdO/SiO_2-Acac; (**b**) $PdO_{0.88}/SiO_2$-Acac; (**c**) $PdO_{0.82}/SiO_2$-Acac; (**d**) $PdO_{0.58}/SiO_2$-Acac. (**B**) Methane conversion versus reaction time over the $PdO_{0.82}/SiO_2$-Acac catalyst; after reaction for 60 h, the catalyst is subjected to a reduction treatment in hydrogen at 400 °C for 1 h and oxidation treatment in air at 350 °C for 0.5 h and then re-tested for lean methane oxidation. The reactions were conducted at 280 °C with the feed of 1 vol.% CH_4 and 99 vol.% air and a GHSV of 30,000 mL h^{-1} g^{-1}.

2.4. More about the Active PdO_x Species in Lean Methane Oxidation

The active phase of Pd in lean methane oxidation is a longstanding puzzle. Some recent studies suggest that Pd^0 is the "most active phase" in lean methane oxidation [9,15]. However, the state of metallic Pd changes gradually along with the reaction course in the oxygen-rich ambiance, and the PdO_x or even PdO species was probably the actual working Pd species in the lean methane oxidation at elevated temperatures [28,29]. Hellman and co-workers observed that the efficient dissociation of methane required sufficiently thick PdO(101) films or metallic Pd [11], consistent with the result of DFT calculation that either under-coordinated Pd sites in PdO and metallic Pd surfaces displayed low activation energies for methane oxidation. This phenomenon was also observed for CO oxidation; multilayer PdO(101) was intrinsically much more active in CO oxidation than the single-layer PdO(101)/Pd(100) [30]. For the lean methane oxidation at a rather low temperature (<300 °C), which is mainly concerned in this work, when the metallic Pd species is exposed to the oxygen-rich atmosphere, a monolayer of Pd oxide may be generated immediately. Along with the reaction course, a Pd oxide shell around the metal core is formed and its thicknesses increase with the increase in reaction temperature and time on stream, and eventually, bulk PdO may be formed [4].

DFT calculation was further performed to elucidate the intrinsic relationship between the reactivity of methane oxidation and the active surface Pd species, as illustrated in Figure S9 of the Supplementary Materials. As the methane molecule is highly stable and has a weak interaction with the catalyst surfaces, the dissociative adsorption of methane is assumed as the rate determining step in the catalytic cycle of methane oxidation. The most stable bulk Pd(100), PdO(100) and three monolayer PdO(101)/Pd(100) (3ML, labeled as

$PdO_{0.75}$, where the atomic ratio of O to Pd is 0.75) are modeled to mimic the surface Pd^0, PdO and PdO_x, respectively, as PdO(101) is the stable surface for an epitaxially grown PdO film on Pd(100) [12,31–33].

The structures of reactant, transition state and product as well as energy change for the dissociative adsorption of methane on the Pd(100), PdO(100) and $PdO_{0.75}$ (3ML-PdO(101)/Pd(100)) surfaces are comparatively presented in Table S2 of the Supplementary Materials. On Pd(100), methane is weakly absorbed; a four-center transition state (H_3C–Pd–H–Pd) is formed upon electron transfer from the carbon–hydrogen bond to the Pd atom, which is further decomposed into Pd–CH_3 and Pd–H. On both 3ML-PdO(101)/Pd(100) and PdO(100), the exposed Pd atom is inserted into a C–H bond of CH_4 and the H atom is concurrently abstracted by the vicinal O species, forming the four-center transition state (H_3C–Pd–H–O), which is then decomposed into Pd–CH_3 and OH. Apparently, the $PdO_{0.75}$ surface exhibits the lowest energy barrier (0.73 eV) and reaction energy (−0.33 eV) for the methane dissociation; in contrast, the PdO(100) surface displays the highest energy barrier (1.27 eV). Meanwhile, although Pd(100) shows a similar energy barrier to $PdO_{0.75}$, the reaction over the former Pd(100) surface is endothermic by 0.53 eV, thermodynamically unfavorable. In addition, Pd(100) is usually shown as O*–Pd(100) with high O coverage, because the adsorption energy of O_2 on Pd(100) is up to −2.0 eV and the energy barrier of O_2 dissociation is only 0.03 eV [31]; nevertheless, the energy barrier for methane dissociation on O*–Pd (100) is 1.0–1.5 eV, still much higher than that on $PdO_{0.75}$ [7]. That is, the DFT calculation results also prove that the PdO_x species is much more active than Pd^0 and PdO in the dissociation of methane.

Notably, Sui and co-workers observed a non-monotonic pressure dependence of the catalytic reaction rate in the range of 0.1–1.2 MPa [34], a behavior contrast to other noble metals (Pt and Rh) where the methane reaction rates always increased with rising pressure. The reactions were conducted at 627 °C and the volume contents of methane and oxygen were 4.9–6.0% and 24.8–40.7%, respectively. Similarly, through first-principle microkinetics modeling, Floren and co-workers observed different pressure dependences of intrinsic TOF at three temperature regimes [35]. At a temperature below 420 °C or above 475 °C, a negative or positive pressure dependency (in the range of 0.1–1.0 MPa) of intrinsic TOF was observed, respectively. In the intermediate temperature regime (420–475 °C), the effect of total pressure on the TOF showed a temperature- and pressure-dependent maximum. Meanwhile, when the impact of mass and heat transport on the TOF was taken into account, the intermediate temperature regime spanned a narrower range of 400–430 °C. Such a non-monotonic pressure dependence behavior was attributed to the pressure-dependent coverages of the dominant surface species such as water, bicarbonates and hydroxyls.

In this work, a series of PdO_x/SiO_2-Acac catalysts with similar Pd particle sizes but different oxidation states was prepared through proper redox treatments, to mimic various Pd species of different valence states in a working catalyst in lean methane oxidation. Their catalytic activity was evaluated at a rather low temperature of 230 °C and atmospheric pressure, to allow no significant change in the Pd state in a short period. Meanwhile, a low methane feed concentration (1 vol.%, dry feed, without co-feeding any H_2O and CO_2) and a low methane conversion (<6%) allow one to have a right evaluation on the intrinsic catalytic activity of various PdO_x species. In this case, the coverage of surface water, bicarbonates and hydroxyls species as well as the impact of mass and heat transport should be rather minor. The results accord well with previous reports that Pd^0 is more active than PdO. Moreover, the catalytic activity is closely related to the oxidation state of PdO_x species (representing by the value of x) and the activity of various Pd species follows the order of $PdO_x \gg Pd > PdO$. The PdO_x/SiO_2-Acac catalysts (in particular for $PdO_{0.82}/SiO_2$-Acac when $x = 0.82$) exhibit much higher activity for lean methane oxidation at low temperature than Pd/SiO_2-Acac and PdO/SiO_2-Acac. As a result, we believe that it is just a coincidence between the non-monotonic dependence of the catalytic activity on the Pd oxidation state observed in this work and the non-monotonic pressure dependence of the catalytic reaction rate reported by Sui, Floren and co-workers [34,35]. In their cases,

it seems that PdO was always the dominant active species during the whole reaction courses, whereas in this work, PdO_x/SiO_2 with different Pd oxidation states was used and the oxidation state of Pd may even change during the reaction course. Two phenomena should be rather different in their intrinsic causation, though both reveal the mechanical complexity of methane oxidation over the supported Pd catalysts.

In addition, for the lean methane oxidation at low temperature, the catalytic activity of PdO_x/SiO_2-Acac is degraded considerably along with the reaction, owing primarily to the over oxidation of PdO_x species. However, such a degradation process is reversible and the reactivity of the spent PdO_x/SiO_2-Acac catalyst can be completely recovered when the oxidation state of PdO species is resumed to original PdO_x through proper redox treatments.

3. Experimental Section

3.1. Catalyst Preparation

The Pd/SiO_2 catalysts were prepared by a simple dry ball-milling method. Fumed silica (SiO_2) supplied by CABOT (CAB-O-SIL M-5, Davisil, with a surface area of $200 \text{ m}^2 \text{ g}^{-1}$ and average particle size of 12 nm) was used as the support. Palladium chloride ($PdCl_2$), nitrate ($Pd(NO_3)_2$), acetate ($Pd(OAc)_2$) and acetylacetonate ($Pd(Acac)_2$) are comparatively employed as the Pd precursor. Prior to mixing with the palladium precursor, the SiO_2 support was treated with dilute nitric acid, washed thoroughly with deionized water several times to ensure a neutral pH value for the filtrate, and then dried overnight at 100 °C. The SiO_2 support was then mixed with the palladium precursor, with a designated Pd loading of 1 wt.%, in a planetary ball mill operated at a rotation speed of 400 rpm for 1 h. The obtained solid was dried overnight at 110 °C and calcined in air at 400 °C for 4 h. The resultant catalysts are designated as Pd/SiO_2-*R*, where *R* is Cl, NO_3, OAc and Acac, representing $PdCl_2$, $Pd(NO_3)_2$, $Pd(OAc)_2$ and $Pd(acac)_2$, respectively, as the Pd precursor.

To probe the most active Pd species, a series of PdO_x/SiO_2-Acac catalysts with different Pd oxidation states was prepared by oxidizing the previously reduced Pd/SiO_2-Acac catalyst at 240–500 °C in air, where *x* is the fraction of PdO, in the range of 0–100%, determined by the Pd 3d XPS results as $x = [PdO]/([Pd] + [PdO])$.

For comparison, another series of $xPdO(1 − x)Pd/SiO_2$-Acac catalysts (*x* = 0–100%) was prepared through following procedures: first, the $Pd(Acac)_2$ precursor was divided into two portions; the first portion $Pd(Acac)_2$ with a fraction of *x* was used to prepare $xPdO/SiO_2$-Acac by the ball-milling method and calcined in air at 400 °C for 3 h; next, the rest of $Pd(Acac)_2$ with a fraction of $1−x$ was introduced to $xPdO/SiO_2$-Acac by ball-milling and then calcined in air at 200 °C for 3 h, to get the $xPdO(1 − x)Pd/SiO_2$-Acac catalysts.

3.2. Catalyst Characterization

X-ray powder diffraction (XRD) patterns were collected on a powder X-ray diffractometer (Bruker AXS D8, Karlsruhe, Germany) with a monochromated Cu Kα radiation source (0.15406 nm, 40 kV, and 40 mA), in the 2θ range of 5–80° with a scanning rate of $4° \text{ min}^{-1}$.

The surface area (BET) of the catalyst sample was measured by N_2 sorption at −196 °C on a physisorption analyzer (Micromeritics TriStar 3000, Norcross, GA, USA); prior to the measurement, the sample was degassed under vacuum at 300 °C for 8 h.

Thermogravimetric analysis (TGA) was carried out on a Thermo plus Evo TG 8120 analyzer (Rigaku Corporation, Osaka, Japan) coupled with an online mass spectrometer; the sample was heated in air from room temperature to 800 °C at a heating rate of $10 °C \text{ min}^{-1}$, during which, the mass loss as well as the MS signals corresponding to H_2O (m/z = 18) and CO_2 (m/z = 44) were monitored.

Inductively coupled plasma-optical emission spectrometry (ICP-OES, Thermo iCAP 6300, Thermo Scientific, Waltham, MA, USA) was used to determine the actual loading of Pd, by dissolving the powdery Pd/SiO_2 catalysts in aqua regia and hydrofluoric acid.

Fourier transform infrared spectroscopy (FT-IR) was measured on an infrared spectrometer (Bruker Vertex 70, Karlsruhe, Germany) by scanning 120 times with a resolution of 4 cm^{-1} and in the range of 400–3100 cm^{-1}.

Transmission electron microscopy (TEM) images of the catalyst sample were obtained on a JEM 2010 microscope (JEOL Ltd., Tokyo, Japan) operating at 200 kV; to prepare the probe sample, the catalyst sample was spread evenly into anhydrous ethanol and then dropped on the copper grid.

X-ray photoelectron spectroscopy (XPS) was performed on a ULVAC PHI-5800 scanning ESCA microprobe electron spectrograph (Physical Electronics Company, Chanhassen, MN, USA) with Al Kα radiation and a multichannel detector. The charging effect was corrected by referencing the binding energy of C 1s at 284.6 eV. The ex situ XPS analysis was measured in parallel with the active tests for the fresh catalysts; both are conducted almost at the same time, in one day after preparation and treatment. The XPS of spent catalysts was measured very shortly after the activity tests. All these can ensure that the XPS spectra collected in this work could well reveal the actual state of the catalysts working in the reactor.

Temperature-programmed reduction by hydrogen (H$_2$-TPR) was performed on a Micromeritics AutoChem II 2920 chemisorption analyzer (Micromeritics, Norcross, GA, USA). About 50 mg catalyst sample was loaded in the sample tube. The H$_2$-TPR profiles were obtained by heating the catalyst sample at a ramp of 10 °C min^{-1} in a flowing 10% H$_2$/Ar stream (30 mL min^{-1}).

3.3. Catalytic Tests

The catalytic tests for methane oxidation were carried out in a fixed-bed reactor at atmospheric pressure. Typically, 200 mg of the catalyst sample (40–60 mesh) was placed in a quartz tube with an internal diameter of 6.0 mm, filled with quartz sand and separated by quartz cotton. The feed gas consisted of 1 vol.% CH$_4$ and 99 vol.% air, with a flow rate of 100 mL min^{-1}, corresponding to a gas hourly space velocity (GHSV) of 30,000 mL h^{-1} g^{-1}.

To evaluate the overall activity of reduced Pd/SiO$_2$ catalyst, the catalyst sample was first reduced in situ with H$_2$ at 400 °C for 1 h. The reactor was then cooled down and stabilized at 50 °C in a N$_2$ flow. After that, the feed gas of 1 vol.% CH$_4$ + 99 vol.% air was introduced through the reactor and the reactor was then heated from 50 °C at a heating rate of 2 °C min^{-1}, until a complete conversion of CH$_4$ was achieved. The products were analyzed online by using a gas chromatograph (GC-2010, Shimadzu corporation, Kyoto, Japan) equipped with a post-column methanator and a flame ionization detector (FID). As only complete oxidation products (CO$_2$ and H$_2$O) were detected in this work and no carbonaceous deposition was observed on the catalyst surface in all catalytic tests, the conversion of CH$_4$ was then calculated by the concentrations of CH$_4$ and CO$_2$ in the effluents as

$$x_{CH_4} = [CO_2]_{out}/([CO_2]_{out} + [CH_4]_{out}) \times 100\%$$

The temperatures corresponding to a methane conversion of 10%, 50%, 90% and 100% are denoted as $T_{10\%}$, $T_{50\%}$, $T_{90\%}$ and $T_{100\%}$, respectively. Meanwhile, as the feed methane concentration used in this work is rather low (1 vol.%), the difference in the flow rate between the feed and effluent streams was also very small (in general <1%). It was then estimated that the mass balance for the experimental tests should be better than 99%.

To determine the activity of Pd/SiO$_2$ with different oxidation states, the reactor was stabilized at 230 °C and the methane oxidation reaction was conducted at this temperature for a period of about 60 min, during which, the conversion of methane was determined at a certain interval. To elucidate the inherent catalytic activity, the turnover frequency (TOF, h^{-1}) was calculated as

$$TOF = \frac{x_{CH_4} \times F \times C_0 \times 60 \times 106.42}{22414 \times w_{cat} \times L_{Pd}}$$

where F is the standard feed flow rate (mL min^{-1}), C_0 is the feed methane concentration (vol.%), w_{cat} is the mass of catalyst loaded in the reactor (g), and L_{Pd} is the loading of Pd in the catalyst (wt.%).

4. Conclusions

A series of Pd/SiO$_2$ catalysts were prepared with different Pd precursors by a dry ball-milling method and used in the oxidation of lean methane at low temperature. The effect of Pd precursors on the catalytic performance of Pd/SiO$_2$ was investigated and the state of the most active Pd species was probed.

The results indicate that the Pd dispersion and catalytic performance of the Pd/SiO$_2$ catalysts prepared by the dry ball-milling method in lean methane oxidation are greatly dependent on the palladium precursor. Among four precursors, viz., palladium chloride (Cl), nitrate (NO$_3$), acetate (OAc) and acetylacetonate (Acac), the catalytic activity of various Pd/SiO$_2$ catalysts follows the order of Pd/SiO$_2$-Acac > Pd/SiO$_2$-OAc > Pd/SiO$_2$-Cl >> Pd/SiO$_2$-NO$_3$. In particular, the Pd/SiO$_2$-Acac catalyst prepared from palladium acetylacetonate displays a high dispersion of Pd species as well as a superior resistance against sintering upon calcination and reduction at high temperature; it exhibits excellent performance in the lean methane oxidation and the temperature corresponding to a methane conversion of 90% is only 288 °C, better than most of those reported in the open literature. Consequently, it seems that dry ball-milling is a simple but rather effective method to prepare the Pd/SiO$_2$ catalysts for lean methane oxidation and palladium acetylacetonate is an ideal precursor to get highly active Pd/SiO$_2$ with well and stably dispersed Pd species.

Besides the size and dispersion of Pd particles, the oxidation state of Pd species also plays a crucial role in determining the catalytic activity of Pd/SiO$_2$ in lean methane oxidation at low temperature. A non-monotonic dependence of the catalytic activity on the Pd oxidation state is observed. The activity of various Pd species follows the order of PdO$_x$ >> Pd > PdO; the PdO$_x$/SiO$_2$-Acac catalysts (in particular for PdO$_{0.82}$/SiO$_2$-Acac when $x = 0.82$) exhibit much higher activity in lean methane oxidation at low temperature than Pd/SiO$_2$-Acac and PdO/SiO$_2$-Acac. The catalytic activity of PdO$_x$/SiO$_2$ may be degraded during the methane oxidation due to the gradual transformation of PdO$_x$ to PdO in the oxygen-rich ambiance; however, such a degradation process is reversible and the activity of a spent Pd/SiO$_2$ catalyst can be completely recovered through a redox treatment to regain the PdO$_x$ species.

The insight shown in this work helps to foster a better understanding of the relationship between the structure and performance of supported Pd catalysts by clarifying the state of active Pd species, which should be beneficial to designing an active catalyst in the lean methane oxidation at low temperature.

Supplementary Materials: The following tables and figures are available online at https://www.mdpi.com/article/10.3390/catal11060725/s1. Table S1. A comparison of various supported palladium catalysts in their activity for lean methane combustion. Table S2. DFT calculated structures of the reactant, transition state, and product for the dissociation of methane over the Pd(100), PdO$_{0.75}$ (3ML-PdO(101)/Pd(100)), and PdO(100) surfaces as well as the corresponding energy barrier ($\Delta E_{int}^{\neq}$, eV) and reaction energy change (ΔE_r, eV). Figure S1. TEM images and Pd particle size distribution curves of the Pd/SiO$_2$-x catalysts prepared by the dry ball-milling method with different Pd precursors calcined at 400, 600 and 800 °C: (a) Pd/SiO$_2$-Acac, (b) Pd/SiO$_2$-OAc, (c) Pd/SiO$_2$-Cl and (d) Pd/SiO$_2$-NO$_3$. Figure S2. FT-IR spectra of the SiO$_2$ support and Pd/SiO$_2$-Acac catalyst. Figure S3. TG-MS profiles of the Pd(Acac)$_2$/SiO$_2$ catalyst: (a) weight loss; (b) DTG curve; (c) H$_2$O signal in effluent; (d) CO$_2$ signal in effluent. Figure S4. Light off tests of lean methane oxidation over the Pd/SiO$_2$-x catalysts prepared by the dry ball-milling method with different Pd precursors (after the ball-milling, the Pd/SiO$_2$ catalysts was calcined in air at 400, 600, and 800 °C, as marked in the legends, for 4 h and then reduced with hydrogen at 400 °C for 1 h): (a) Pd/SiO$_2$-Acac, (b) Pd/SiO$_2$-OAc, (c) Pd/SiO$_2$-Cl; and (d) Pd/SiO$_2$-NO$_3$. Figure S5. (A) XRD patterns of the Pd/SiO$_2$-Acac catalysts that come through the lean methane oxidation reaction at different temperatures: (a) original; (b) 200 °C; (c) 220 °C; (d) 240 °C; (e) 260 °C; (f) 280 °C; (g) 300 °C; (h) 320 °C. (B) XRD patterns

of the xPdO+(1−x)Pd/SiO$_2$-Acac catalysts, a mixture of PdO/SiO$_2$-Acac and Pd/SiO$_2$-Acac with different contents of PdO: (a) Pd/SiO$_2$-Acac; (b) 0.2PdO+0.8Pd/SiO$_2$-Acac; (c) 0.4PdO+0.6Pd/SiO$_2$-Acac; (d) 0.6PdO+0.4Pd/SiO$_2$-Acac; (e) 0.8PdO+0.2Pd/SiO$_2$-Acac; (f) PdO/SiO$_2$-Acac. Figure S6. Pd 3d XPS spectra of the PdO$_x$/SiO$_2$-Acac catalysts with different Pd oxidation states obtained by oxidizing the previously reduced Pd/SiO$_2$-Acac in air for 30 min at different temperatures: (a) fresh reduced Pd/SiO$_2$-Acac; (b) 240 °C; (c) 250 °C; (d) 300 °C; (e) 350 °C; (f) 400 °C; (g) 500 °C; (h) calcined PdO/SiO$_2$-Acac. Figure S7. TEM images and Pd particle size distribution curves of the PdO$_x$/SiO$_2$-Acac catalysts with different Pd oxidation states (obtained by oxidizing the previously reduced Pd/SiO$_2$-Acac in air for 30 min at different temperatures): (a) Pd/SiO$_2$-Acac; (b) PdO$_{0.36}$/SiO$_2$-Acac; (c) PdO$_{0.58}$/SiO$_2$-Acac; (d) PdO$_{0.75}$/SiO$_2$-Acac; (e) PdO$_{0.82}$/SiO$_2$-Acac; (f) PdO$_{0.88}$/SiO$_2$-Acac; (g) PdO$_{0.95}$/SiO$_2$-Acac; (h) PdO/SiO$_2$-Acac. Figure S8. TEM images (A), Pd particle size distribution curve (B) and Pd 3d XPS spectra (C) of the spent PdO$_{0.82}$/SiO$_2$-Acac catalyst come through lean methane oxidation reaction at 280 °C for 60 h. Figure S9. Models of the most stable bulk PdO(100), Pd(100), and three monolayer PdO(101)/Pd(100) (3ML, labeled as PdO$_{0.75}$, where the atomic ratio of Pd and O is 0.75).

Author Contributions: Conceptualization, Z.Q., Z.W. and J.W.; project management, M.D., W.F. and J.W.; methodology and investigation, L.Y., C.F., L.L., Z.W., Z.Q., W.F. and J.W.; DFT calculation, Y.C. and L.Y.; visualization, L.Y., Z.Q. and Y.C.; writing—original draft preparation, L.Y. and Z.Q.; writing—review and editing, Z.Q. and J.W.; funding acquisition, Z.W. and J.W.; supervision, Z.Q., M.D. and W.F. All authors have read and agreed to the published version of the manuscript.

Conflicts of Interest: The authors declare no conflict of interest.

References

1. He, L.; Fan, Y.; Bellettre, J.; Yue, J.; Luo, L. A review on catalytic methane combustion at low temperatures: Catalysts, mechanisms, reaction conditions and reactor designs. *Renew. Sust. Energy Rev.* **2020**, *119*, 109589. [CrossRef]
2. Jiang, X.; Mira, D.; Cluff, D. The combustion mitigation of methane as a non-CO$_2$ greenhouse gas. *Prog. Energy Combust. Sci.* **2018**, *66*, 176–199. [CrossRef]
3. Monai, M.; Montini, T.; Gorte, R.J.; Fornasiero, P. Catalytic Oxidation of Methane: Pd and Beyond. *Eur. J. Inorg. Chem.* **2018**, *2018*, 2884–2893. [CrossRef]
4. Su, S.; Carstens, J.; Bell, A.T. A Study of the Dynamics of Pd Oxidation and PdO Reduction by H$_2$ and CH$_4$. *J. Catal.* **1998**, *176*, 125–135. [CrossRef]
5. Willis, J.; Gallo, A.; Sokaras, D.; Aljama, H.; Nowak, S.; Goodman, E.; Wu, L.; Tassone, C.; Jaramillo, T.; Abild-Pedersen, F.; et al. Systematic Structure–Property Relationship Studies in Palladium-Catalyzed Methane Complete Combustion. *ACS Catal.* **2017**, *7*, 7810–7821. [CrossRef]
6. Lupescu, J.; Schwank, J.; Fisher, G.; Hangas, J.; Peczonczyk, S.; Paxton, W. Pd model catalysts: Effect of air pulse length during redox aging on Pd redispersion. *Appl. Catal. B Environ.* **2018**, *223*, 76–90. [CrossRef]
7. Chin, Y.; García-Diéguez, M.; Iglesia, E. Dynamics and Thermodynamics of Pd–PdO Phase Transitions: Effects of Pd Cluster Size and Kinetic Implications for Catalytic Methane Combustion. *J. Phys. Chem. C* **2016**, *120*, 1446–1460. [CrossRef]
8. Bychkov, V.; Tulenin, Y.; Slinko, M.; Khudorozhkov, A.; Bukhtiyarov, V.; Sokolov, S.; Korchak, V. Self-oscillations of methane oxidation rate over Pd/Al$_2$O$_3$ catalysts: Role of Pd particle size. *Catal. Commun.* **2016**, *77*, 103–107. [CrossRef]
9. Chen, J.; Zhong, J.; Wu, Y.; Hu, W.; Qu, P.; Xiao, X.; Zhang, G.; Liu, X.; Jiao, Y.; Zhong, L.; et al. Particle Size Effects in Stoichiometric Methane Combustion: Structure–Activity Relationship of Pd Catalyst Supported on Gamma-Alumina. *ACS Catal.* **2020**, *10*, 10339–10349. [CrossRef]
10. Liu, C.; Lin, C.; Chen, J.; Lu, K.; Lee, J.; Chen, J. SBA-15-supported Pd catalysts: The effect of pretreatment conditions on particle size and its application to benzyl alcohol oxidation. *J. Catal.* **2017**, *350*, 21–29. [CrossRef]
11. Hellman, A.; Resta, A.; Martin, N.; Gustafson, J.; Trinchero, A.; Carlsson, P.; Balmes, O.; Felici, R.; Van Rijn, R.; Frenken, J. The Active Phase of Palladium during Methane Oxidation. *J. Phys. Chem. Lett.* **2012**, *3*, 678–682. [CrossRef] [PubMed]
12. Martin, N.; Van den Bossche, M.; Hellman, A.; Grönbeck, H.; Hakanoglu, C.; Gustafson, J.; Blomberg, S.; Johansson, N.; Liu, Z.; Axnanda, S.; et al. Intrinsic Ligand Effect Governing the Catalytic Activity of Pd Oxide Thin Films. *ACS Catal.* **2014**, *4*, 3330–3334. [CrossRef]
13. Nilsson, J.; Carlsson, P.; Fouladvand, S.; Martin, N.; Gustafson, J.; Newton, M.; Lundgren, E.; Grönbeck, H.; Skoglundh, M. Chemistry of Supported Palladium Nanoparticles during Methane Oxidation. *ACS Catal.* **2015**, *5*, 2481–2489. [CrossRef]
14. Simplício, L.; Brandão, S.; Sales, E.; Lietti, L.; Bozon-Verduraz, F. Methane combustion over PdO-alumina catalysts: The effect of palladium precursors. *Appl. Catal. B Environ.* **2006**, *63*, 9–14. [CrossRef]

15. Xiong, H.; Wiebenga, M.; Carrillo, C.; Gaudet, J.; Pham, H.; Kunwar, D.; Oh, S.; Qi, G.; Kim, C.; Datye, A. Design considerations for low-temperature hydrocarbon oxidation reactions on Pd based catalysts. *Appl. Catal. B Environ.* **2018**, *236*, 436–444. [CrossRef]

16. Doan, H.; Sharma, M.; Epling, W.; Grabow, L. From Active-Site Models to Real Catalysts: Importance of the Material Gap in the Design of Pd Catalysts for Methane Oxidation. *ChemCatChem* **2017**, *9*, 1594–1600. [CrossRef]

17. Burch, R.; Urbano, F. Investigation of the active state of supported palladium catalysts in the combustion of methane. *Appl. Catal. A Gen.* **1995**, *124*, 121–138. [CrossRef]

18. Lin, W.; Zhu, Y.; Wu, N.; Xie, Y.; Kemnitz, E. Total oxidation of methane at low temperature over $Pd/TiO_2/Al_2O_3$: Effects of the support and residual chlorine ions. *Appl. Catal. B Environ.* **2004**, *50*, 59–66. [CrossRef]

19. Nassreddine, S.; Bergeret, G.; Jouguet, B.; Geantet, C.; Piccolo, L. Operando study of iridium acetylacetonate decomposition on amorphous silica–alumina for bifunctional catalyst preparation. *Phys. Chem. Chem. Phys.* **2010**, *12*, 7812–7820. [CrossRef] [PubMed]

20. Womes, M.; Lynch, J.; Bazin, D.; Le Peltier, F.; Morin, S.; Didillon, B. Interaction between $Pt(acac)_2$ and alumina surfaces studied by XAS. *Catal. Lett.* **2003**, *85*, 25–31. [CrossRef]

21. Hu, X.; Schuster, J.; Schulz, S.; Gessner, T. Surface chemistry of copper metal and copper oxide atomic layer deposition from copper (II) acetylacetonate: A combined first-principles and reactive molecular dynamics study. *Phys. Chem. Chem. Phys.* **2015**, *17*, 26892–26902. [CrossRef]

22. Nasibulin, A.; Kauppinen, E.; Brown, D.; Jokiniemi, J. Nanoparticle Formation via Copper (II) Acetylacetonate Vapor Decomposition in the Presence of Hydrogen and Water. *J. Phys. Chem. B* **2001**, *105*, 11067–11075. [CrossRef]

23. Danielis, M.; Colussi, S.; de Leitenburg, C.; Soler, L.; Llorca, J.; Trovarelli, A. Outstanding Methane Oxidation Performance of Palladium-Embedded Ceria Catalysts Prepared by a One-Step Dry Ball-Milling Method. *Angew. Chem. Int. Ed.* **2018**, *57*, 10212–10216. [CrossRef]

24. Santo, V.; Sordelli, L.; Dossi, C.; Recchia, S.; Fonda, E.; Vlaic, G.; Psaro, R. Characterization of Pd/MgO Catalysts: Role of Organometallic Precursor–Surface Interactions. *J. Catal.* **2001**, *198*, 296–308. [CrossRef]

25. Van Veen, J.; De Jong-Versloot, M.; Van Kessel, G.; Fels, F. A thermoanalytic-mass spectrometric study of oxide-supported acetyl acetonates. *Thermochim. Acta* **1989**, *152*, 359–370. [CrossRef]

26. Wu, Z.; Zhang, C.; Peng, L.; Wang, X.; Kong, Q.; Gu, X. Enhanced Stability of MFI Zeolite Membranes for Separation of Ethanol/Water by Eliminating Surface Si-OH Groups. *ACS Appl. Mater. Inter.* **2018**, *10*, 3175–3180. [CrossRef]

27. Farrauto, R.; Hobson, M.; Kennelly, T.; Waterman, E. Catalytic chemistry of supported palladium for combustion of methane. *Appl. Catal. A Gen.* **1992**, *81*, 227–237. [CrossRef]

28. Xu, J.; Ouyang, L.; Mao, W.; Yang, X.; Xu, X.; Su, J.; Zhuang, T.; Li, H.; Han, Y. Operando and Kinetic Study of Low-Temperature, Lean-Burn Methane Combustion over a $Pd/\gamma\text{-}Al_2O_3$ Catalyst. *ACS Catal.* **2012**, *2*, 261–269. [CrossRef]

29. Mahara, Y.; Tojo, T.; Murata, K.; Ohyama, J.; Satsuma, A. Methane combustion over $Pd/CoAl_2O_4/Al_2O_3$ catalysts prepared by galvanic deposition. *RSC Adv.* **2017**, *7*, 34530–34537. [CrossRef]

30. Mehar, V.; Kim, M.; Shipilin, M.; Van den Bossche, M.; Gustafson, J.; Merte, L.; Hejral, U.; Grönbeck, H.; Lundgren, E.; Asthagiri, A.; et al. Understanding the Intrinsic Surface Reactivity of Single-Layer and Multilayer PdO (101) on Pd (100). *ACS Catal.* **2018**, *8*, 8553–8567. [CrossRef]

31. Jørgensen, M.; Grönbeck, H. First-Principles Microkinetic Modeling of Methane Oxidation over Pd (100) and Pd (111). *ACS Catal.* **2016**, *6*, 6730–6738. [CrossRef]

32. Rogal, J.; Reuter, K.; Scheffler, M. Thermodynamic stability of PdO surfaces. *Phys. Rev. B* **2004**, *69*, 075421. [CrossRef]

33. Seriani, N.; Harl, J.; Mittendorfer, F.; Kresse, G. A first-principles study of bulk oxide formation on Pd (100). *J. Chem. Phys.* **2009**, *131*, 054701. [CrossRef]

34. Sui, R.; Mantzaras, J.; Es-sebbar, E.; Bombach, R. Hetero-/homogeneous combustion of fuel-lean $CH_4/O_2/N_2$ mixtures over PdO at elevated pressures. *P. Combust. Inst.* **2019**, *37*, 5465–5472. [CrossRef]

35. Florén, C.R.; Van den Bossche, M.; Creaser, D.; Grönbeck, H.; Carlsson, P.A.; Korpic, H.; Skoglundhand, M. Modelling complete methane oxidation over palladium oxide in a porous catalyst using firstprinciples surface kinetics. *Catal. Sci. Technol.* **2018**, *8*, 508–520. [CrossRef]